SATELLITE MEASUREMENTS OF ATMOSPHERIC OZONE PROFILES, INCLUDING TROPOSPHERIC OZONE, FROM ULTRAVIOLET/VISIBLE MEASUREMENTS IN THE NADIR GEOMETRY: A POTENTIAL METHOD TO RETRIEVE TROPOSPHERIC OZONE

K. V. CHANCE,[a] J. P. BURROWS,[b] D. PERNER,[c] and W. SCHNEIDER[d]

[a]Harvard-Smithsonian Center for Astrophysics, 60 Garden Street, Cambridge, MA 02138, U.S.A.,
[b]Institute of Remote Sensing, University of Bremen, Bremen, Germany, [c]Atmospheric Chemistry Division,
Max Planck Institute for Chemistry, Mainz, Germany, and [d]Euromap GmbH, Neustrelitz, Germany

Abstract—Numerical studies of a new method for the retrieval of ozone profile information from nadir-observing satellite measurements in the ultraviolet and visible are presented. The method combines information from back scattered radiation in the Hartley band down to the O_3 concentration peak, lower atmospheric information from the temperature structure of the Huggins bands, and a constraint on the total column from the Chappuis bands. The Huggins bands' temperature structure provides altitude information on the ozone distribution that includes clear distinction between stratospheric and tropospheric ozone. Studies presented here include dependence of the retrieved O_3 profiles on surface albedo, tropospheric aerosol, and tropospheric O_3 content for a range of atmospheric conditions. Published by Elsevier Science Ltd

1. INTRODUCTION

The importance of the stratospheric ozone layer to terrestrial life and the need for precise long-term monitoring of the stratospheric ozone climatology are well established. Ozone also plays a significant role in the chemistry of the troposphere, where its photolysis leads to the production of OH, the most important tropospheric oxidizing agent.[1] Haagen-Smit et al[2] showed that the production of tropospheric ozone is dependent on the presence of hydrocarbons, oxides of nitrogen, and light. Crutzen[3] elucidated the mechanism for the HO_x- and NO_x-catalysed photochemical generation of ozone in the troposphere. The first experimental evidence that tropospheric ozone may be increasing was reported from balloon-sonde observations made between 1967 and 1982 at the meteorological station on Hohenpeissenberg in southern Germany.[4] An analysis of ozone measurements made at the clean air stations of Mauna Loa, Hawaii and Point Barrow, Alaska agreed with this finding and indicated an average increase of ozone of 0.5–1.5% per year during the period 1974–1989 with the largest increases occurring during summer.[5] Volz and Kley[6] investigated the ozone measurement technique used by Albert-Lévy and co-workers at Montsouris, near Paris, in the late 19th and early 20th centuries and concluded that the method is reliable.[7,8] These data indicate that the ozone mixing ratio in clean air was about 10 ppbv at the end of the last century near Paris. Present day surface measurements are a factor of 2–4 larger. As a result of such observations, concern about the impact of tropospheric ozone pollution is rapidly growing. To accurately assess the importance of these changes, global measurements of the distribution of tropospheric ozone are required.

Due to the relatively short lifetime and consequent variability of tropospheric ozone, measurements made by satellite-borne remote sensing instruments are the most efficient way to obtain global information on its distribution. A key difficulty in spaceborne monitoring of tropospheric ozone is the ability of the measurements and the retrieval approach to distinguish the contribution of stratospheric ozone from that of tropospheric ozone in the detected signals. A

method to determine the vertical distribution of stratospheric ozone by monitoring back scattered radiation in the ultraviolet Hartley and Huggins bands of ozone was first proposed by Singer and Wentworth in 1957,[9] and has been successfully applied by the BUV instrument on *Nimbus* 4 and the SBUV instrument on *Nimbus* 7.[10,11] SBUV obtains stratospheric profile information from the differing scattering depths, as well as the total ozone column, by measuring at 12 selected wavelength bands in the range 256–340 nm. The SBUV instrument uses relatively wide (1 nm) wavelength bands that do not resolve the fine structure of the ozone absorption. Stratospheric ozone vertical profiles, with limited geographical coverage, have also been obtained successfully using solar occultation by the SAGE I and II instruments.[12]

A method is presented here for remote sensing of ozone profiles, including tropospheric ozone, from orbiting spectrometers which measure upwelling atmospheric radiation between 240 and 800 nm. This study includes simulation of several viewing scenarios, as well as realistic estimation of instrument performance derived from studies for the Global Ozone Monitoring Experiment (GOME) and the SCanning Imaging Absorption spectroMeter for Atmospheric CHartographY (SCIAMACHY), since demonstrated by GOME, to infer the precision of the technique. The present work was instrumental in establishing the GOME and SCIAMACHY instrument programs, by demonstrating that nadir-looking instruments can measure tropospheric ozone globally. GOME is a European Space Agency instrument launched on the European Remote Sensing 2 satellite in April 1995. It is a nadir mapping instrument that views the Earth with continuous wavelength coverage from 240 to 790 nm at a resolution of 0.2 nm in the ultraviolet and 0.4 nm in the visible.[13–15] SCIAMACHY is a German/Dutch/Belgian instrument which is part of the payload for the ESA Envisat-1 Polar Platform, currently scheduled for launch in 1999. SCIAMACHY is an enhanced version of GOME having, in addition to nadir viewing, limb and occultation measuring modes, and extended wavelength coverage to 2.4 μm.[16–18]

2. SPECTROSCOPIC METHOD

The Huggins bands of ozone have discrete vibrational structure between 300 and 370 nm, with features having widths significantly less than 1 nm. This is the sharpest known vibrational structure of any electronic band of O_3. This structure has a strong temperature dependence due to the onset of thermal population of excited vibrational levels in the electronic ground state (see measurements in Refs. 19 and 20). It is this temperature-dependent structure that provides a spectral signature for tropospheric O_3; its differential character derives from the onset with increasing temperature of the weaker vibrational hot-band absorption between the stronger absorption peaks, which are due to absorption from $O_3(000)$.

The ozone measurement technique presented here includes the measurement of the Hartley, Huggins, and Chappuis bands at moderately high resolution (ca. 0.2 nm in the Hartley and Huggins bands, ca. 0.4 nm in the Chappuis bands). In addition to providing more continuous wavelength coverage for deriving information on vertical profiles from the scattering depth, it permits the use of the temperature structure of the Huggins bands to increase the altitude profile information. In particular, since tropospheric ozone is significantly warmer than stratospheric ozone at any altitude in the stratosphere where there is significant O_3, tropospheric ozone column amounts are cleanly separated from the stratospheric column. The Chappuis bands are temperature independent and occur at visible wavelengths where light penetrates to the ground under favorable meteorological conditions. Thus, their measurement provides improved total column O_3 information to the measurement set.

3. RADIANCE AND RETRIEVAL CALCULATIONS

3.1. Forward radiance model

Radiance calculations are performed for the present studies using the AFGL LOWTRAN7 radiance code.[21] The version of the code used here includes the correction of all recently discovered errata [G. P. Anderson and L. W. Abreu, private communications (1989–1992)]. The only modifications made to the code are to increase the number of significant figures for total radiance

provided by the code and for ozone concentrations read in by the code. All calculations are performed using the provided option for multiple scattering employing the k-distribution method.[22]

Calculations use a 12 layer (13 level) model atmosphere, including O_3, H_2O, and O_2, with concentrations from the AFGL atmospheric constituent profiles;[23] their model 6 atmosphere, with pressure and temperature corresponding to the U.S. Standard Atmosphere, is used. This model has a tropopause height of 15 km: subsequent references to tropospheric and stratospheric ozone refer to the column from 0 to 15 km and from 15 to 60 km, respectively (the error due to inclusion of the small mesospheric column, 50–60 km, with the stratosphere is negligible for present purposes). Calculations in this paper are performed for a satellite instrument in a polar orbit with a 10:00 a.m. crossing time, looking vertically down, at 45°N, for two viewing scenarios and tropospheric O_3 distributions: (1) vernal equinox, solar zenith angle = 53.5°, ground level O_3 mixing ratio = 40 ppbv ("normal" tropospheric ozone). In this case, the tropospheric ozone column is 63 Dobson units (DU, 1 DU = 2.687×10^{16} cm^{-2}) and the stratospheric column 276 DU; (2) summer solstice, solar zenith angle = 48.9°, ground level O_3 mixing ratio = 120 ppbv (corresponding to a boundary layer pollution episode under anticyclonic conditions). In this case, the tropospheric ozone column is 76 DU, and the stratospheric column 276 DU. The two ozone distributions are shown in Figs 1(a–h), along with the retrieved O_3 results described below. Contributions from minor interfering atmospheric species are not included in the present calculations. In the ultraviolet these include BrO, H_2CO, and SO_2. Measurements of these species simultaneous with ozone determinations, implying the appropriate correction of the spectra for analysis of ozone absorption, is intended. For example, stratospheric SO_2, greatly enhanced by the eruption of El Chichon, was measured by both the TOMS and SBUV instruments on Nimbus 7.[24–26] Clearly, the presence of interfering species, even when they are included in the retrieval process, will increase the uncertainty in derived ozone over that calculated here. The major interference for the Chappuis bands is from NO_2 and H_2O. These can both be readily corrected for, since the overlaps with the broad Chappuis bands are only partial, and since detailed study of the wavelength-dependent absorption by the Chappuis bands is not necessary; only their absorption in portions of the bands, cleanly separated from interfering species, is necessary to provide column O_3 measurements.

The studies include albedos of 0.3 (typical land value) and 0.02 (sea surface minimum) as specified in the input to LOWTRAN7. They also include rural and urban tropospheric aerosol extinction (IHAZE = 1 and 5 in LOWTRAN7). All studies have been done with the background stratospheric aerosol (IVULCN = 0 in LOWTRAN7). Clear sky conditions are assumed. The limitations to tropospheric ozone measurements due to cloud coverage are currently being studied extensively in the context of the GOME and SCIAMACHY satellite algorithm development. These studies include the knowledge of penetration depth of solar radiation into clouds gained from measurements in the oxygen A bands.[27–29]

3.2. Instrument modeling

The instrument model used in the present studies is a simple one developed in the preliminary stages of instrument and algorithm design for the GOME and SCIAMACHY projects. The instrument is assumed to measure the atmospheric spectrum over the O_3 regions at 0.2 nm resolution from 240 to 350 nm, and at 0.4 nm resolution from 400 to 800 nm (GOME and SCIAMACHY both include the 350–400 nm region as well, negligible for O_3; the GOME coverage ends at 790 nm, a negligible correction to the coverage in the present study). Spectra calculated with LOWTRAN7 are converted to the nanometer scale, appropriate for our measurements with dispersive instruments, and are corrected for resolution and for instrument parameters as follows: etendue = 5.0×10^{-5} cm^2 sr; instrument throughput = 0.15 for $\lambda \leqslant 400$ nm, = 0.20 for $\lambda > 400$ nm; detector quantum efficiency = 0.5; nadir sampling time = 1.5 sec (the GOME default nadir sampling time is 30 sec for $\lambda \leqslant 312$ nm and 1.5 sec for $\lambda > 312$ nm; for simplicity, and as a worst-case scenario, the present study is made using 1.5 sec sampling throughout the GOME wavelength range).

Synthetic noise is added to spectra calculated with the forward model for retrieval study purposes using the Box–Muller method for generating random deviates with a Gaussian distribution.[30] Noise sources include readout noise (10^3 e$^-$/pixel), dark current noise (10^2 e$^-$/pixel), photon statistics, and digitization noise. The digitization noise is calculated assuming 16-bit conversion, with gain factors
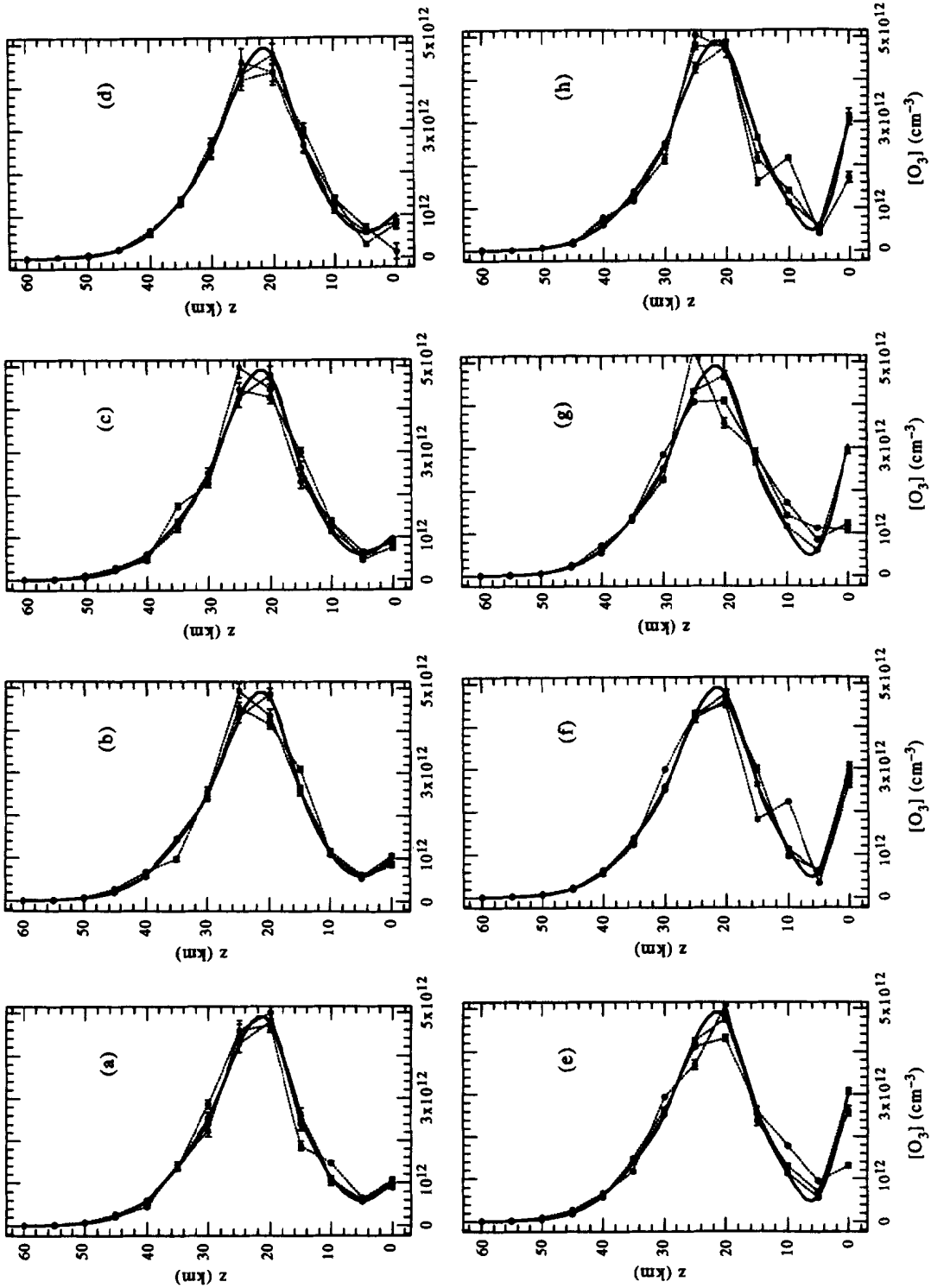
Fig. 1. The results of the fitting study for each of the eight atmospheric scenarios, and for three sets of initial concentrations for each scenario are shown. (——) are the modeled ozone concentrations. Retrieved values include 2σ fitting errors. The atmospheric scenarios are: (a) normal tropospheric ozone, rural haze, albedo 0.3; (b) normal tropospheric ozone, urban haze, albedo 0.3; (c) normal tropospheric ozone, rural haze, albedo 0.02; (d) normal tropospheric ozone, urban haze, albedo 0.02; (e) enhanced tropospheric ozone, rural haze, albedo 0.3; (f) enhanced tropospheric ozone, urban haze, albedo 0.3; (g) enhanced tropospheric ozone, rural haze, albedo 0.02; (h) enhanced tropospheric ozone, urban haze, albedo 0.02.

set appropriate to GOME measurements under conditions of maximum input. These range from 1.0×10^4 photons per pixel for $268 \leqslant \lambda < 312$ nm to 9.0×10^7 photons per pixel for $400 \leqslant \lambda < 800$ nm. Figure 2 is an example of the forward calculation, with noise added, corresponding to the measurement case with 40 ppbv tropospheric ozone, albedo $= 0.3$, and the rural haze model.
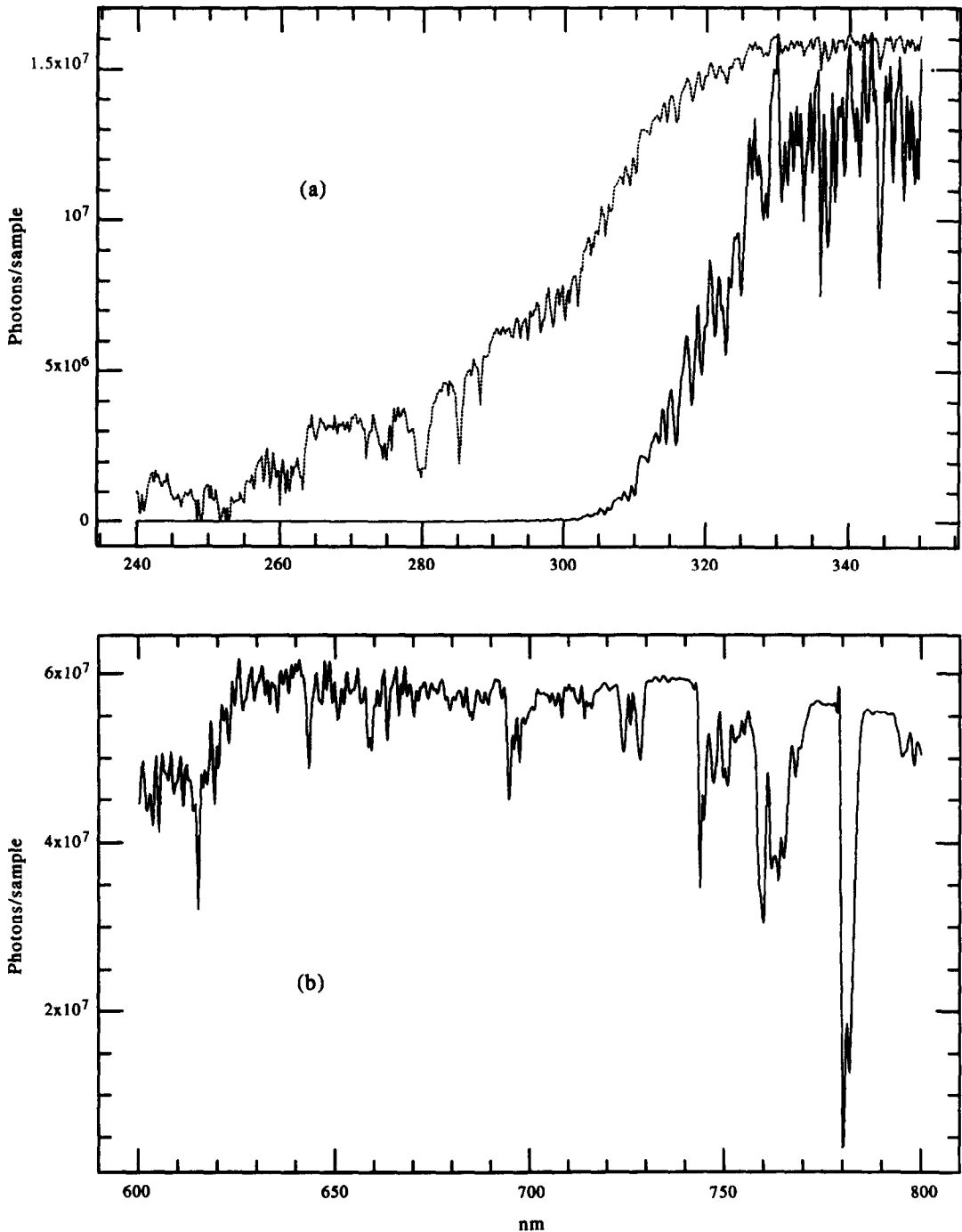
Fig. 2. An example of the forward calculation, with noise added, corresponding to the scenario with 40 ppbv tropospheric ozone, albedo $= 0.3$, and the rural haze model: (a) the Hartley–Huggins band region. Because of the large dynamic range of the spectrum its logarithm is also plotted (. . . .); (b) the Chappuis band region.

3.3. Retrieval studies

Figure 3 shows the ozone absorption cross sections for the Hartley, Huggins, and Chappuis bands at a representative temperature for the peak of the stratospheric ozone layer (220 K). These are calculated at the GOME/SCIAMACHY spectral resolution. The TOMS and standard (step
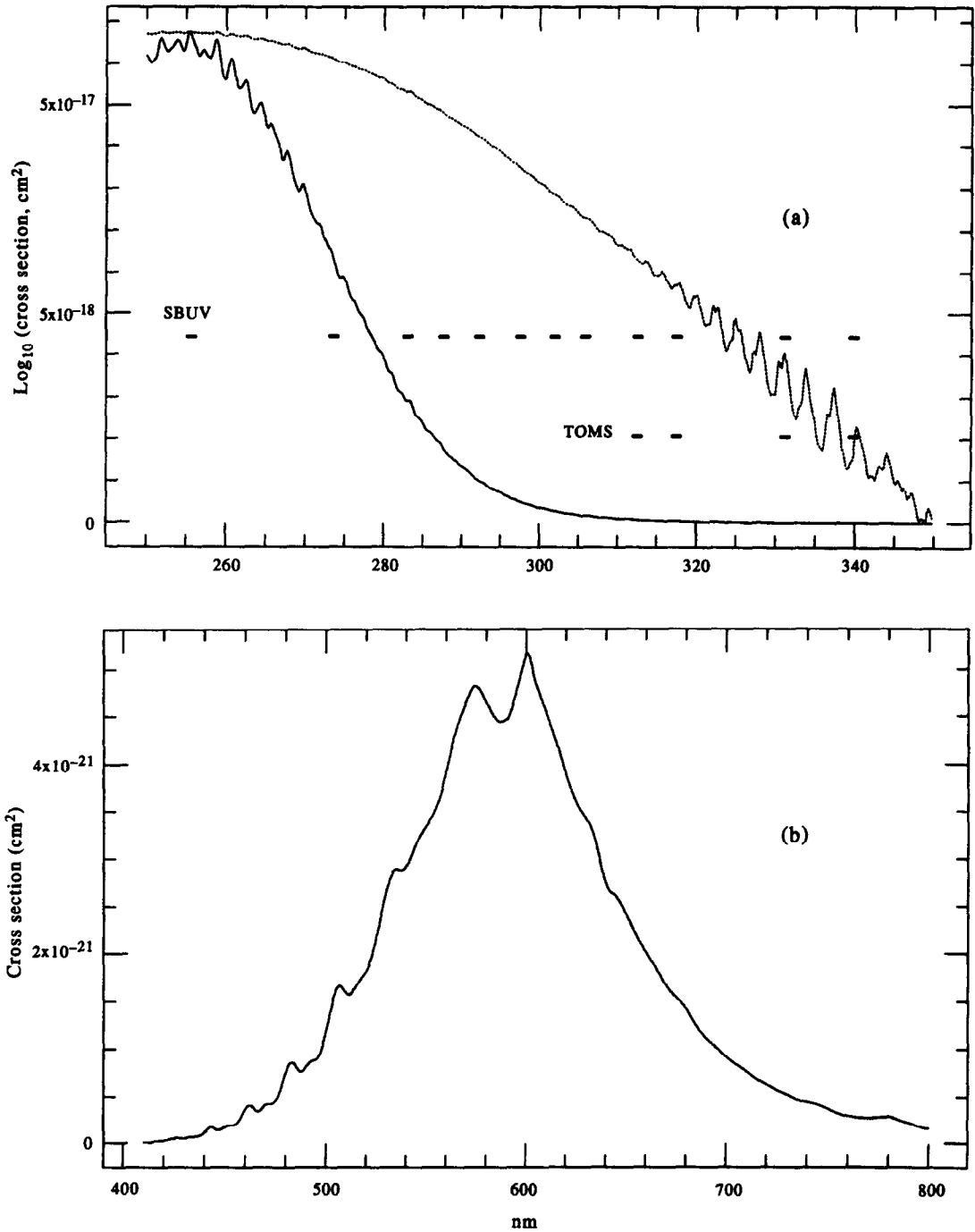
Fig. 3. Ozone absorption cross sections calculated at the GOME/SCIAMACHY spectral resolution. (a) The Hartley and Huggins bands at a representative temperature for the peak of the stratospheric ozone layer (220 K). The TOMS and standard (step scan mode) SBUV wavelength bands are also shown (TOMS also has channels at 360 and 380 nm). The strong variation in the strength for u.v. absorption, together with the approximate λ^4 dependence of the Rayleigh scattering, provides for discrimination of O_3 at different altitudes from the measurement of back scattered light at different wavelengths. (b) The Chappuis bands.
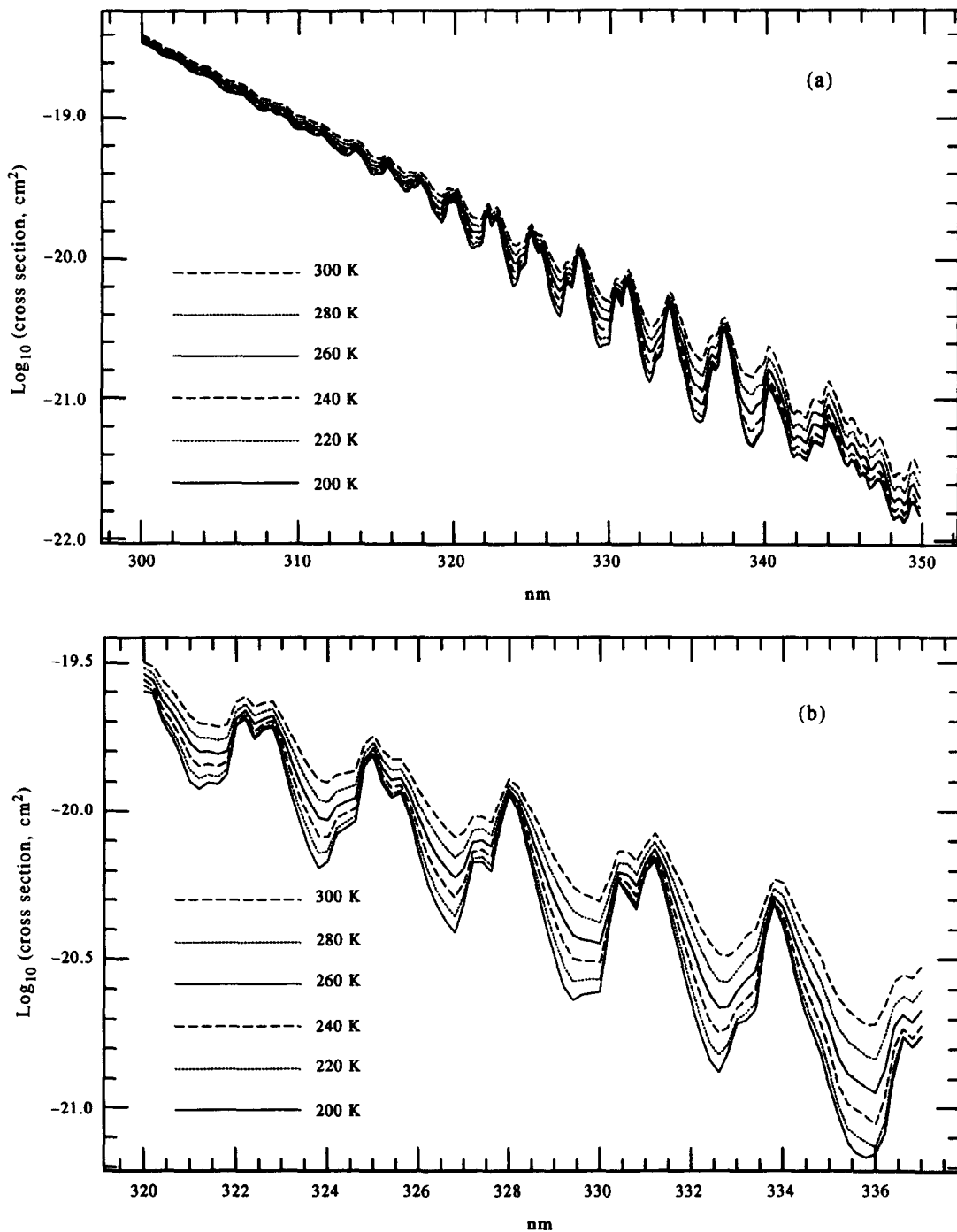
Fig. 4. (a) Temperature dependent cross sections in the O_3 Huggins bands calculated from the parameterization in the LOWTRAN7 code over the stratospheric and tropospheric ozone temperature range; (b) the same cross sections as Fig. 4(a), but only over the 320–337 nm range, to illustrate details of the temperature dependence in the region of primary importance for determination of tropospheric ozone.

scan mode) SBUV wavelength bands are also shown in the figure. The strong variation in the strength for u.v. absorption, together with the appropriate λ^4 dependence of the Rayleigh scattering, provides for discrimination of O_3 at different altitudes from the measurement of back scattered light at different wavelengths.

Precise measurements have been made of the temperature dependence of the Huggins bands from 300 to 340 nm.[19,20] The values of the cross sections derived from these measurements currently used

in the AFGL LOWTRAN7 radiance code are shown in Fig. 4(a) for the range of temperatures relevant to atmospheric ozone measurements. Less precise measurements exist to wavelengths longward of 340 nm, in the weaker part of the Huggins bands, and efforts are currently underway to provide precise laboratory measurements there as well. Figure 4(b) shows the same cross sections as Fig. 4(a), but only over the 320–337 nm range. The portion of the Huggins bands longward of 320 nm is the region of primary importance for determination of tropospheric ozone.

Calculated forward spectra, including the instrument model and noise, are generated as described in Sec. 3.2. Fitting studies are then performed on these synthetic spectra using the non-linear least squares technique.[31] Such an input spectrum is generated, with instrument parameters and noise, for each set of input conditions. These include (as detailed in Sec. 3.1) two choices of viewing scenario and ozone profile ("normal" and "polluted" troposphere), two choices of albedo (land surface average and sea surface minimum), and two choices of tropospheric aerosol distribution (rural and urban), for a total of eight input scenarios studied. The non-linear least-squares fitting analysis is then performed by allowing the O_3 concentration at each of the 13 atmospheric levels to vary independently in the forward model calculation while iterating to minimize the difference between the forward model calculation and the pre-computed forward spectrum plus noise. Iteration is continued until the calculated spectrum agrees in the least-squares sense with the input spectrum to within a specified χ^2 criterion or until all input parameters have stopped varying to within preset, small, amounts. Fitting is performed for each of the eight input scenarios, using three initial O_3 distributions. These are: (1) the normal input O_3 distribution; (2) the normal input O_3 distribution multiplied by 0.75, corresponding to 254 DU total ozone; and (3) the normal input O_3 distribution multiplied by 1.125, corresponding to 423 DU total ozone.

Non-linear least-squares fitting of data is not anticipated to be a part of the normal retrieval procedure for determination of O_3 profiles from satellite data; far too much computational time is required, even on advanced computers. This type of study has been used during the investigative phase of the GOME and SCIAMACHY to determine the maximal information that can be obtained from satellite measurements. Algorithm studies now being conducted include, among other elements, the use of look-up tables and the optimal estimation method[32,33] to design an efficient and accurate algorithm for retrieval of atmospheric gas amounts, including O_3 profiles, from the satellite measurements.

4. RESULTS AND DISCUSSION

Figures 1(a–h) shows the results of the fitting study for each of the eight input scenarios, and for the three sets of initial concentrations for each scenario. The concentrations for the input spectra and the 2σ fitting errors are included in the figure. Table 1 gives the integrated total ozone columns, as well as the tropospheric (i.e., $\leqslant 15$ km) and stratospheric (> 15 km) columns, and their uncertainties, as derived from the fitting analysis.

The relative fitting uncertainties for tropospheric, stratospheric, and total ozone columns are substantially less than those for the individual derived levels. There is substantial correlation between ozone derived for adjacent levels, particularly in the troposphere. This is evident from examination of the correlation matrices derived in the least-squares fitting procedure (used to determine the uncertainties in the column amounts). There is also some suggestion of alternating behavior in fitting to adjacent altitude levels in Fig. 1. The fitting to the scenarios with enhanced tropospheric ozone shows a tendency to underestimate the ozone at the lowest altitude, compensating by placing it higher in the troposphere. The 5 km altitude resolution chosen for tropospheric retrievals in this study is probably near to the limit of what is feasible. An exception to this may be for ozone in a warm boundary layer where the temperature-induced contrast in the Huggins bands will be particularly pronounced. The U.S. Standard Atmosphere temperature and pressure profile used in these studies includes a very broad tropopause region (11–20 km). When atmospheric conditions with steeper temperature gradients in the tropopause region are encountered, ozone profiles might be retrievable to higher effective altitude resolution.

The ability to retrieve ozone profile information depends upon knowledge of the atmospheric temperature profile. The requirements for this knowledge have not been determined in the present study. Temperature knowledge to ± 5 K is estimated to be adequate, but this needs to be quantified

Table 1. Tropospheric, stratospheric, and total O_3 column retrievals.

Conditions			Normal tropospheric ozone[†]			Enhanced tropospheric ozone[†]		
			Troposphere	Stratosphere	Total	Troposphere	Stratosphere	Total
"True" profile			62.8	275.5	338.3	76.0	275.5	351.5
Albedo	Haze	Starting profile[‡]						
0.30	rural	1.00	61.9 ± 0.9	276.1 ± 0.6	337.9 ± 0.3	75.9 ± 0.5	275.6 ± 0.4	351.5 ± 0.2
0.30	rural	1.25	59.9 ± 1.1	277.5 ± 0.8	337.5 ± 0.5	78.1 ± 0.8	273.2 ± 0.7	351.2 ± 0.4
0.30	rural	0.75	63.8 ± 0.8	273.7 ± 0.6	337.4 ± 0.4	85.8 ± 0.5	267.3 ± 0.3	353.2 ± 0.2
0.30	urban	1.00	61.7 ± 0.6	276.2 ± 0.4	337.9 ± 0.4	76.0 ± 0.4	275.5 ± 0.3	351.5 ± 0.3
0.30	urban	1.25	63.2 ± 0.7	275.2 ± 0.5	338.4 ± 0.3	75.2 ± 0.5	275.8 ± 0.3	351.0 ± 0.3
0.30	urban	0.75	63.3 ± 0.5	274.1 ± 0.3	337.4 ± 0.3	76.8 ± 0.5	267.0 ± 0.2	343.8 ± 0.3
0.02	rural	1.00	62.4 ± 0.9	275.4 ± 0.7	337.8 ± 0.5	76.5 ± 0.5	275.1 ± 0.2	351.6 ± 0.3
0.02	rural	1.25	64.7 ± 1.0	274.0 ± 0.7	338.7 ± 0.5	83.2 ± 0.6	267.6 ± 0.3	350.8 ± 0.4
0.02	rural	0.75	64.3 ± 0.6	272.8 ± 0.5	337.1 ± 0.4	82.5 ± 0.6	268.4 ± 0.4	350.8 ± 0.5
0.02	urban	1.00	61.9 ± 1.0	275.5 ± 0.7	337.4 ± 0.9	76.0 ± 0.7	275.5 ± 0.4	351.5 ± 0.6
0.02	urban	1.25	60.9 ± 2.4	272.7 ± 0.7	333.6 ± 2.6	75.5 ± 0.8	274.6 ± 0.5	350.3 ± 0.7
0.02	urban	0.75	61.5 ± 0.8	272.6 ± 0.5	334.1 ± 0.7	71.0 ± 0.8	268.2 ± 0.5	339.3 ± 0.8

[†]2σ retrieval errors are given.
[‡]Multiplier for initial conditions (× "true" profile with normal tropospheric ozone).

in further studies. Limited retrievals were also performed using only the Hartley and Huggins band region, eliminating the Chappuis bands. In these cases, the uncertainties for tropospheric, stratospheric, and total ozone columns were about a factor of 10 higher. An attempt was made to retrieve profiles using only the Hartley band but, as expected, there was negligible sensitivity to lower atmospheric ozone.

5. CONCLUSION

It has been shown that nadir measurements of the ozone Hartley, Huggins, and Chappuis bands at sufficient spectral resolution to resolve the structure provides information on the altitude distribution of ozone, including tropospheric ozone. Altitude resolution in the troposphere is limited to ca. 5 km, except in special conditions. The studies here are limited to clear sky conditions; in practice, information could be derived down to the scattering height. These studies contributed to the decisions to produce several satellite instruments for atmospheric measurements. The first of these, GOME, is now operating successfully in orbit, producing data that should soon confirm the level to which this type of retrieval can be carried out practically.

Table 1 shows that the derived stratospheric and tropospheric ozone columns are cleanly separated to quite good precision, even with the caveat given above for strong correlation at the 5 km altitude resolution scale in the troposphere. Thus, under clear sky conditions, separate stratospheric and tropospheric columns are obtainable to high precision to within the limitations of the present study. While we do not anticipate that complete global coverage for tropospheric ozone will be routinely achieved by the satellite measurements we are undertaking, due chiefly to interference in the observations by clouds, we are confident that measurements of its global climatology will be greatly enhanced by these satellite measurements.

This type of measurement and analysis should also substantially improve the determination of the climatology of stratospheric ozone, since the interference in measurements by tropospheric ozone, including the confusion in analysis caused by the masking of tropospheric ozone by clouds, is removed by the clean separation achieved between stratospheric and tropospheric ozone determinations.

The studies for retrieval of ozone and other constituents from the GOME and SCIAMACHY instruments are currently in process. Clearly, the work discussed here is preliminary in the sense that many further atmospheric and instrumental complications, as well as details of retrieval theory, must be considered before a full retrieval procedure can be finalized. Practical application may well be limited by systematic effects, such as the uncertainty in radiometric calibration. The

results presented here are, however, an encouraging example of the power of utilizing modern array detector technology in satellite instruments for atmospheric constituent measurements. These efforts should lead to substantial improvement in the determination of the global distributions of ozone and other gases.

REFERENCES

1. H. Levy, *Science* **173**, 141 (1971).
2. A. J. Haagen-Smit, E. F. Darley, M. Zaitlin, H. Hull, and W. Noble, *Plant Physio.* **27**, 18 (1951).
3. P. J. Crutzen, *Pure Appl. Geophys.* **106–108**, 1385 (1973).
4. W. Attmannspacher, R. Hartmannnsgruber, and P. Lang, *Meteorol. Rdsch.* **37**, 193 (1984).
5. S. J. Oltmans, W. D. Komhyr, P. R. Franchois, and W. A. Mathews, in *Ozone in the Atmosphere*, D. Bojkov and P. Fabian, eds. A. Deepak, Hampton, VA (1989).
6. A. Volz and D. Kley, *Nature* **332**, 240 (1988).
7. Albert-Lévy, *Annuaire de l'Observ. de Montsouris*, pp. 495–505, Gauthier-Villars, Paris (1878).
8. P. Miguel, *Annls. Obs. Mun.* **11**, 6 (1910).
9. S. F. Singer and R. C. Wentworth, *J. Geophys. Res.* **62**, 299 (1957).
10. D. F. Heath, A. J. Krueger, H. A. Roeder, and B. D. Henderson, *Opt. Eng.* **14**, 323 (1975).
11. J. E. Frederick, R. P. Cebula, and D. F. Heath, *J. Clim. Appl. Meteorol.* **24**, 904 (1985).
12. M. P. McCormick, J. M. Zawodny, R. E. Veiga, J. C. Larsen, and P. H. Wang, *Plan. Space Sci.* **37**, 1567 (1989).
13. J. P. Burrows, P. J. Crutzen, K. Chance, J. C. Geary, F. Goutail, G. W. Harris, G. K. Moortgat, C. Muller, D. Perner, U. Platt, J.-P. Pommereau, W. Schneider, and P. Simon, *SCIAMINI*, Max Planck Institut für Chemie, 55122 Mainz, Germany (1988).
14. K. V. Chance, J. P. Burrows, and W. Schneider, *Proc. S.P.I.E., Remote Sensing of Atmospheric Chemistry* **1491**, 151 (1991).
15. J. P. Burrows, K. V. Chance, A. P. H. Goede, R. Guzzi, B. J. Kerridge, C. Muller, D. Perner, U. Platt, J.-P. Pommereau, W. Schneider, R. J. Spurr, and H. van der Woerd, *Global Ozone Monitoring Experiment Interim Science Report*, T. D. Guyenne and C. Readings, eds. Report ESA SP-1151, ESA Publications Division, ESTEC, Noordwijk, The Netherlands, ISBN 92-9092-041-6 (1993).
16. J. P. Burrows, K. V. Chance, P. J. Crutzen, H. van Dop, J. C. Geary, T. J. Johnson, G. W. Harris, I. S. A. Isaksen, G. K. Moortgat, C. Muller, D. Perner, U. Platt, J.-P. Pommereau, H. Rodhe, E. Roeckner, W. Schneider, H. Sundqvist, and J. Vercheval, *The SCIAMACHY Project—A European Proposal for Atmospheric Remote Sensing*. Max Planck Institute für Chemie, 55122 Mainz, Germany (1988).
17. J. P. Burrows, W. Schneider, J. C. Geary, K. V. Chance, A. P. H. Goede, H. J. M. Aarts, J. de Vries, C. Smorenburg, and H. Visser, *Digest of Topical Meeting on Optical Remote Sensing of the Atmosphere*, Vol. 4, pp. 71–74, Optical Society of America, Washington, DC (1990).
18. J. P. Burrows and K. V. Chance, *Proc. S.P.I.E., Future European and Japanese Remote Sensing Sensors and Programs* **1490**, 146 (1991).
19. A. M. Bass and R. J. Paur, in *Atmospheric Ozone, Proceedings of the Quadrennial Ozone Symposium*, C. Zerefos and A. Ghazi, eds., pp. 606–616, D. Reidel, Hingham, MA (1985).
20. K. Yoshino, D. E. Freeman, J. R. Esmond, and W. H. Parkinson, *Planet. Space Sci.* **36**, 395 (1988).
21. F. X. Kneizys, E. P. Shettle, L. W. Abreu, J. H. Chetwynd, G. P. Anderson, W. O. Gallery, J. E. A. Selby, and S. A. Clough, *Users Guide to LOWTRAN7*, AFGL-TR-88-0177, AD A206773 (1988).
22. R. G. Isaacs, W.-C. Wang, R. D. Worsham, and S. Goldenberg, *Appl. Opt.* **26**, 1272 (1987).
23. G. Anderson, S. Clough, F. Kneizys, J. Chetwynd, and E. Shettle, Environmental Research Papers, No. 954, AFGL-TR-86-0110 (1986).
24. A. J. Krueger, *Science* **220**, 1377 (1983).
25. R. D. McPeters, D. F. Heath, and B. M. Schlesinger, *Geophys. Res. Lett.* **11**, 1203 (1984).
26. G. J. S. Bluth, S. D. Doiron, C. C. Schnetzler, A. J. Krueger, and L. S. Walter, *Geophys. Res. Lett.* **19**, 151 (1992).
27. J. Fischer and H. Grassl, *J. Appl. Meteorol.* **30**, 1245 (1991).
28. J. Fischer, W. Cordes, A. Schmitz-Peiffer, W. Renger, and P. Mörl, *J. Appl. Meteorol.* **30**, 1260 (1991).
29. A. Kuze and K. V. Chance, *J. Geophys. Res.* **99**, 14,481 (1994).
30. W. Press, B. Flannery, S. Teukolsky, and W. Vetterling, *Numerical Recipes*, Chap. 7, Cambridge Univ. Press, New York, NY (1986).
31. D. Marquardt, *J. Soc. Indust. Appl. Math.* **11**, 431 (1963).
32. C. Rodgers, *Rev. Geophys. Space Phys.* **14**, 609 (1976).
33. R. Munro, Middle atmosphere water vapour, Ph.D. thesis, Oxford Univ. (1991).